Co-adsorption of Fluoride and Hydroxide Ions on Ag(111) in Alkaline Electrolytes: Electrochemical and SHG Studies

By M. Danckwerts[1], E. R. Savinova[1,2,3,*], S. L. Horswell[1], B. Pettinger[1], and K. Doblhofer[1]

[1] Fritz-Haber-Institut der Max-Planck-Gesellschaft, Faradayweg 4–6, 14195 Berlin, Germany
[2] Boreskov Institute of Catalysis, Russian Academy of Sciences, Pr. Akademika Lavrentieva 5, 630090 Novosibirsk, Russian Federation
[3] Present address: Technische Universität München, Physik-Department E19, James-Franck-Str. 1, 85748 Garching, Germany

Dedicated to Prof. Dr. Dieter M. Kolb on the occasion of his 60th birthday

Hydroxide (OH^-) adsorption at Ag(111)/alkaline electrolyte interfaces is the initial step leading to the formation of surface oxide. We investigate how OH^- anion adsorption is influenced by co-adsorption of supporting electrolyte anions (F^-). Pure NaF and NaOH as well as mixed electrolytes ranging from pH = 5.8 to 14 are investigated. The rotational anisotropy of the second harmonic generation (SHG) signal is measured to distinguish adsorptive processes from structural changes on the Ag surface. Our results clearly show a cross-over from F^--dominated to OH^--dominated adsorption, while both species remain charged upon adsorption. At more positive potentials, but below the reversible potential of bulk oxide growth, OH is discharged leading to sub-monolayer oxide build-up, whereas in acidic electrolyte, Ag is dissolved. At intermediate pH, the formation of a structured OH^-/F^- co-adsorbed layer is proposed.

1. Introduction

Anion adsorption at metal/electrolyte interfaces is one of the central issues of fundamental electrochemistry. Specifically adsorbed ions affect the reactivity

---

* Corresponding author. E-mail: savinova@ph.tum.de

of metal surfaces; this is of practical importance in electrocatalysis, electrosynthesis and metal dissolution/deposition. Hydroxide adsorption is of particular interest, since it can lead to the formation of a variety of surface species, ranging from chemisorbed anions to discharged OH_{ads}, O_{ads} and ultimately metal oxide, depending on the electrode potential and metal chemistry. Each of the above species may influence the chemistry at the electrode/electrolyte interface in a different way and can drastically change the rates of interfacial processes. This has been documented for example for oxygen and hydrogen peroxide reduction on gold [1, 2] and has been proposed also for silver electrodes [3–5].

The present article continues our efforts in the investigation of a Ag(111) surface in alkaline electrolytes. We use optical second-harmonic generation (SHG) to obtain *in situ* information on the electric field distribution at the electrode/electrolyte interface and the symmetry of the substrate. In our previous studies, we showed that on Ag(111) in an alkaline electrolyte, adsorbed OH^- anions undergo a transition to discharged O species, which ultimately leads to formation of surface oxide [6]. Despite the investigations performed by our and other groups using electrochemical techniques [5, 7–12], XPS [13–15], STM [16] and SERS [17, 18], some details of the hydroxide adsorption on Ag and the initial stages of surface oxidation are still not fully understood. In particular, these concern (i) the bonding of hydroxide to the substrate and the controversial question of charge transfer during hydroxide adsorption, (ii) the influence of co-adsorbed supporting electrolyte anions on the hydroxide adsorption and surface oxidation, and (iii) the possible structure of the adlayer. In this paper we address the question of how OH^- adsorption and oxide formation is influenced by competitive F^- adsorption. We use cyclic voltammetry and *in situ* second-harmonic generation (SHG) to investigate the electrochemical and structural characteristics of Ag(111) electrodes in mixed NaF/NaOH electrolytes at various pH.

2. Experiment and sample preparation

The Ag(111) crystal (99.999%) was obtained from Mateck and was oriented to better than $0.4°$. Surface finishing was performed by chemical etching in NaCN $+ H_2O_2$ and successive hydrogen flame annealing under a gentle Ar stream using a procedure similar to one described earlier [6, 19]. The specimen was transferred to the electrochemical cell in ultrapure water and immersed into the electrolyte under potential control. Special care was taken that contact of the crystal with air was minimized.

The cyclic voltammetry as well as SHG measurements were carried out in a spectroelectrochemical cell made of Kel-F with an optical window at the bottom. This cell setup combines optical measurements with simultaneous CV in the hanging meniscus configuration, allowing for voltammetric monitoring at

any point of the experiment. All optical adjustments are made while the sample is in contact with the electrolyte and under potentiostatic control; this way the time between preparation of the crystal and its immersion is kept at a minimum. Details of the cell setup have been published elsewhere [6, 20]. The cell allows rotation of the sample around its surface normal to measure the SHG anisotropy. The cell was equipped with a counter electrode made of a Pt-wire ring concentric to the working electrode and a Hg/HgO/0.1M NaOH reference electrode whose potential is $0.165\,V_{NHE}$. Before each experiment, the cell was cleaned in NH_3/H_2O_2 (1:1); at the beginning of an experiment, the cell was purged with Ar.

For the optical measurements, a Nd:YAG laser was used to produce 5 ns laser pulses at the fundamental wavelength of 1064 nm and with ∼150 mJ each pulse. In all experiments presented here, both for the ingoing and the SHG beam the polarizations were selected to be parallel to the reflection plane (pp configuration). Behind the cell, the reflected fundamental beam was blocked by a combined color-glass/interference-filter setup, while the SH radiation was detected with a photomultiplier tube. A computer was used to control the experiment and process the data. In anisotropy measurements, the SHG intensity is recorded as a function of rotational angle; from the anisotropy data, the isotropic and three-fold symmetry coefficients of the surface are obtained [21].

3. Results and discussion

To investigate the influence of varying hydroxide concentrations on the adsorption of OH^- and subsequent formation of surface oxide, cyclic voltammetry (CV) and SHG experiments were carried out in mixed NaF/NaOH electrolyte solutions, where the concentrations were varied such that the ionic strength was kept constant: $(0.1 - x)$ mol/l NaF + x mol/l NaOH, $0 \le x \le 0.1$. The pH of the solutions varied from 5.8 to 13.8, where only the most alkaline solution had an ionic strength of 1 mol/l.

Representative current-voltage characteristics at selected pH are shown in Fig. 1. The shape of the CV in 0.1 M NaOH is consistent with data reported in the literature [22]. A broad peak can be observed at around $-0.5\,V$ *vs.* Hg/HgO, labelled as (a) in Fig. 1. The cathodic scan shows the symmetric counterpart. Based on our previous *ex situ* XPS and *in situ* SHG results [6, 20] and in accordance with other researchers [22–24], this peak has been attributed to the specific adsorption of hydroxide anions:

$$OH^- \rightleftharpoons OH_{ads}^- . \tag{1}$$

In the following, region (a) of any of the presented CVs will therefore be denoted as "adsorption peak".

As the potential is cycled further anodic, but still remains below the reversible Ag_2O formation, between 0 and 0.1 V the current rises a second time.
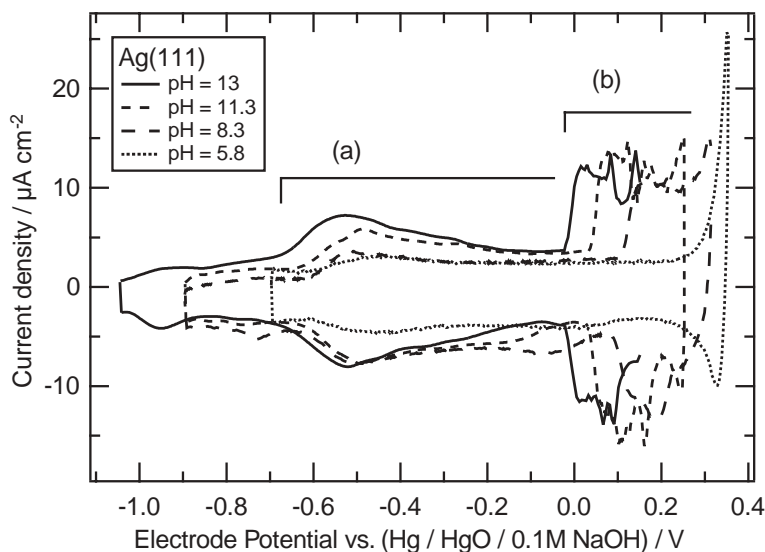
Fig. 1. Cyclic voltammograms of Ag(111) in mixed NaF/NaOH electrolytes at various pH. Solid line: pH = 13, short-dashed line: pH = 11.3, long-dashed line: pH = 8.3, dotted line: pH = 5.8 (NaF + HF). Region (a) is characterized by anion adsorption, region (b) denotes underpotential oxidation.

XPS-examinations of electrodes emersed from the electrolyte in this potential range showed the appearance of O (BE $528.2 \pm 0.2\,\mathrm{eV}$) and Ag^+ (BE $367.7\,\mathrm{eV}$), which was attributed to the formation of Ag_2O underpotential surface oxide:

$$2OH^-_{ads} + 2Ag \rightarrow Ag_2O_{surf} + H_2O + 2e^- \,. \tag{2}$$
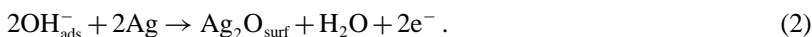
Consequently, the potential region labelled (b) in Fig. 1 is denoted as "oxidation" throughout this paper.

Both processes proved to be sensitive to changes in pH. It can be seen in Fig. 1 that the adsorption peak (a) exhibits a negative shift with increasing pH, accompanied by a rise in the current, indicating an increase in the extent of specific adsorption. For a quantitative investigation, we have defined the onset of the adsorption current as the potential at which the inflexional tangent on the current rise intersects the extrapolated base current at potentials negative to the adsorption. The pH-dependence of this onset is shown in Fig. 2(a). For the most alkaline electrolytes (pH values between 12 and 14), the onset shifts by $(50 \pm 7)\,\mathrm{mV}$ per pH unit as determined from a line fit to the data, which is close to $59\,\mathrm{mV/pH}$ expected for reaction (1) and is in line with earlier publications [22]. However, as the pH is decreased below 12, the dependence levels off. The onset of the adsorption peak is constant in the pH interval from 10 to 6,
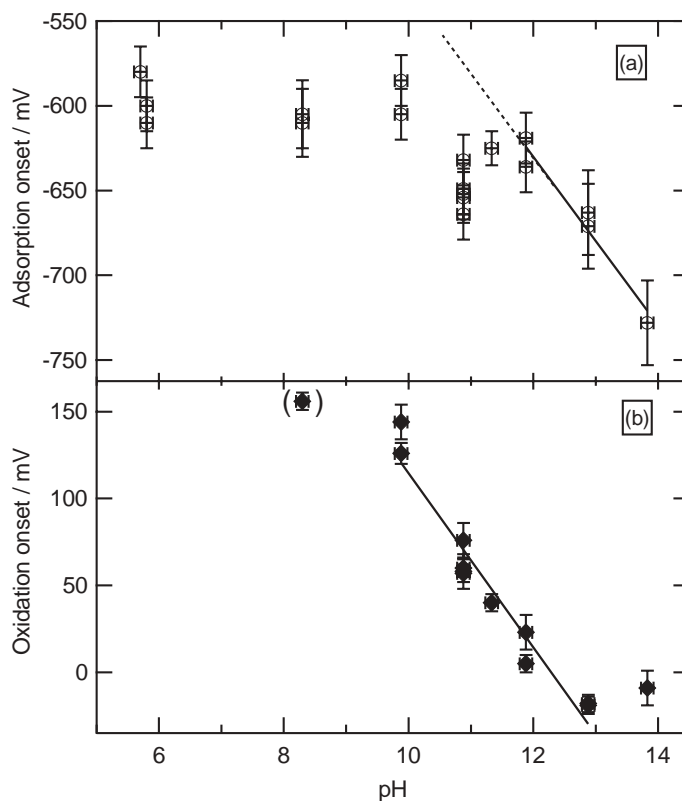
Fig. 2. (a) Onset potential of anion adsorption *vs.* electrolyte pH. The onset potential was determined from the intersection of the inflexional tangent on the current rise with the linear extrapolation of the current before the adsorption. Solid line: linear fit to the data between pH = 11.9 and 13.8 indicating a shift of $-(50\pm7)$ mV/pH. (b) Onset potential of the oxide formation *vs.* pH. A line fit to the data between pH = 9.9 and 12.9 (solid line) yields a shift of $-(60\pm5)$ mV/pH. The data point at pH = 8.3 lacked reproducibility due to possible local pH changes.

where it occurs at *ca.* -0.61 V *vs.* Hg/HgO, corresponding to the point of zero charge (E_{pzc}) of Ag(111) in NaF electrolyte (-0.69 V *vs.* SCE [25]). In the whole pH range studied, prolonged continuous potential cycling did not cause any change of the position of peak (a), proving that it was not sensitive to local pH modulations.

From this behavior we infer that the adsorption feature in the CV corresponds mainly to the adsorption of OH^- at the high pH limit, whereas it is dominated by the adsorption of F^- from the supporting electrolyte at low pH values. There has been some controversy as to whether or not fluoride adsorbs specifically on silver single crystalline faces [26, 27]. In more recent studies,

Valette [28] and Doubova *et al.* [29, 30] provided strong evidence for F⁻ specific adsorption on Ag(111) using capacitance measurements. Vitanov *et al.* also discuss the adsorption of F⁻ as being specific [31]. In any case, fluoride adsorption is weaker than for any other halide ion, comparable to that of small soluble organic molecules [30]. Adding very little amounts of OH⁻ considerably increases the adsorption current, since OH⁻ is more strongly adsorbed. At high pH, the adsorption is fully dominated by hydroxide, as proven by the shift of approximately 60 mV/pH. Thus, the analysis of the onset potential yields three adsorption regions: (i) "pure" hydroxide adsorption in the pH interval from 14 to *ca.* 12, (ii) "pure" fluoride adsorption in the pH interval from *ca.* 6 to 10 and (iii) the intermediate region, where co-adsorption of both ions takes place. The conclusion on fluoride-dominated adsorption in a pH range from 6 to 10 is in line with the observation of Doubova *et al.* [30], who found that capacitance-potential curves for an Ag(111) electrode in NaF/KPF$_6$ electrolyte were identical at pH $= 5.5$ and pH $= 8.3$.

There has been some controversy concerning the pH dependence of OH⁻ adsorption, which is sometimes interpreted as an evidence of ion discharge. Hence, from a shift of 60 mV/pH of the adsorption peak Jovic *et al.* [22] deduce complete charge transfer between OH⁻ ions and the silver surface. Meanwhile, Savinova *et al.* [6] and Danckwerts *et al.* [20], who observe similar pH dependencies, conclude on the absence of charge transfer between hydroxide ions and the metal. Comprehensive discussions of the thermodynamics of specific adsorption are given in a number of publications [32]; however, some brief explanation may be necessary here. Let us consider reaction (1). At equilibrium, the electrochemical potentials of dissolved and adsorbed OH⁻ ions are equal:

$$\bar{\mu}_{OH^-}^{Sol} = \bar{\mu}_{OH^-}^{Ads} \ . \tag{3}$$

Assuming that specifically adsorbed OH⁻ is located at the inner Helmholtz plane (IHP), its electrochemical potential is given by:

$$\bar{\mu}_{OH^-}^{Ads} = \mu_{OH^-}^{Ads}(\theta) + zF\varphi^{IHP} \ , \tag{4}$$

where φ^{IHP} is the electrostatic potential at the IHP, $\mu_{OH^-}^{Ads}(\theta)$ is the coverage dependent chemical potential of adsorbed OH⁻ and z is the charge number of the anion. From this it is evident that the potential drop between the solution and the IHP is a function of the activity of OH⁻ in solution:

$$\varphi^{IHP} - \varphi^{Sol} = \frac{\mu_{OH^-}^{Sol} - \mu_{OH^-}^{Ads}(\theta)}{zF} + \frac{RT}{zF}\ln a_{OH^-} \ . \tag{5}$$

Since φ^{IHP} is related to the electrostatic potential of the metal phase, Eq. (5) accounts for the pH dependence of the adsorption peak. Obviously, specific adsorption of anions is concentration dependent even if they retain their charge.

This has indeed been observed experimentally in a number of cases. We refer here to a recent publication by Kolics and Wieckowski, who observed pronounced shift in the sulfate adsorption peak, along with strong evidence of the absence of Faradaic charge transfer during this process [33].

The variation of the total charge of specifically adsorbed anions σ^- with potential can be concluded from the charge density on the metal $|\sigma_{Ag}| = |\sigma^-| - |\sigma^+|$, where σ^+ is the charge density of co-adsorbed cations in the double layer. Assuming that neither F$^-$ nor OH$^-$ is discharged upon adsorption [6], the charge density on the metal can be obtained from the CV data by integration. The charge under peak (a) then corresponds to the charge flow through the external circuit due to electron removal from the Ag electrode upon anion specific adsorption. This assumption will be verified later by comparing voltammetric and SHG data. The charge has been computed via integration of the anodic sweeps of the CVs. The current densities in different electrolytes merge together[1] at -0.8 V, thus no anion specific adsorption is expected at this point. Consequently, the charge on the electrode at this potential is assumed to be equal in all electrolytes used here. The electrode charge at -0.8 V was calculated by back-integration of the current in 0.1 M NaF starting at $E_{pzc} = -0.61$ V$_{HgO}$ yielding a charge of $-9.8\ \mu$C cm^{-2}. All charge curves for different electrolytes have been obtained by integration from -0.8 V and corrected for this charge.

The total charge densities computed by integration between -0.8 V and various end potentials are plotted in Fig. 3 as a function of pH. Increasing the pH clearly leads to a considerable rise in the metal charge. In the pH region from 6 to 10, the variation is rather small; from 10 to 13, however, it becomes more pronounced. The dotted line shows the charge as calculated from integration up to the respective onset of oxidation. The charge grows as the end potential of the integration is increased, showing that the ion coverage at the Ag surface continues to rise up to the onset of oxidation. In the lower pH range, the overall metal charge is predominantly compensated by fluoride. Around pH $= 10$, there is a crossover from fluoride-dominated to hydroxide adsorption, similar to the observation in Fig. 2. Thus, the charge strongly depends on pH due to hydroxide adsorption in the higher pH range.

The formation of sub-monolayer oxide, observed in the voltammograms as a steep current rise in region (b), also depends on pH. Fig. 2(b) shows the onset potential of surface oxidation as a function of pH. It can be seen that the oxidation onset shifts by approximately 60±5 mV/pH in the pH interval between pH $= 10$ and 13, as obtained from a line fit to the data. This is similar to the adsorption onset as seen in Fig. 2(a). However, a strong deviation considerably exceeding the experimental error is observed at pH $= 14$, where the oxidation onset potential reaches a saturation. This effect confirms our previ-

---

[1] Some differences in the current densities at the negative end of the CVs are due to traces of oxygen. The CVs were corrected for oxygen reduction prior to integration.
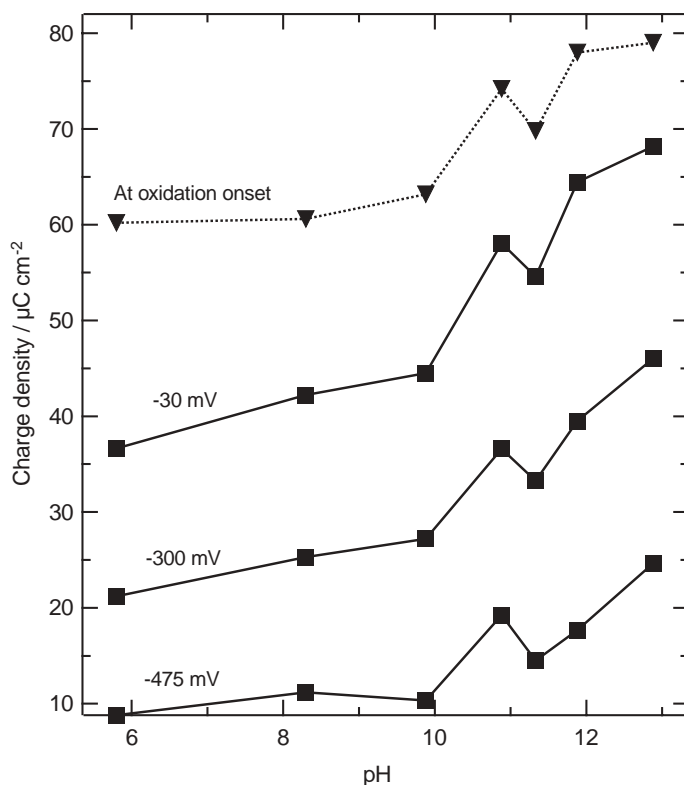
Fig. 3. Metal charge density, calculated from integrating the current, as a function of pH. The integration was started at −0.8 V. The potentials given are the end points of the integration. Dotted line: the current was integrated up to the respective onset of oxidation at each distinct pH.

ous assumption that sub-monolayer surface oxide is formed from an adsorbed OH^{-} intermediate (Eq. (2)) rather than from dissolved hydroxide ions. Indeed, it is reasonable to expect that the dependence of the OH^{-} coverage on the Ag surface (θ_{OH}) on the bulk solute OH^{-} concentration saturates at the high pH limit, being linear at lower concentrations (pH 10–13). At pH = 8.3, peak (b) appeared non-reproducible (in contrast to the adsorption onset), apparently due to local pH changes; it is given in Fig. 2 in brackets.

Varying the pH to acidic changes the electrode behavior at oxidation potentials completely: as can be seen in Fig. 1 for the curve at pH = 5.8 (dotted line), the reversible anodic and cathodic maxima in potential region (b) are lost. Instead, the CV shows a steep anodic increase on the anodic and an irreversible peak on the cathodic scan. These features are typical for a Ag dissolution and deposition process observed in acidic electrolytes. A Pourbaix' diagram for sil-

ver suggests that the transition from silver oxidation to silver dissolution takes place around pH $= 6$ [34].

The adsorption-onset potential at pH 10.9 and 11.3 deviated from the general pH dependence. Since the data point at pH 10.9 was intentionally reproduced repeatedly, it can be ruled out that the discrepancy be due to experimental error. This may point to a specific structure formed during co-adsorption of fluoride and hydroxide anions, which is more stable than those for fluoride- or hydroxide-dominated adsorption. Further studies are needed to confirm this hypothesis.

In the SHG experiments, the anisotropy of the SH intensity is measured; from this the isotropic and 3-fold contributions A and D, respectively, are computed. In Fig. 4(a) the isotropic and 3-fold contributions to the SHG signal of Ag(111) in 0.1 M NaOH (pH $= 13$) are plotted as a function of electrode potential, together with the anodic scan of the corresponding cyclic voltammogram. The isotropic term A grows as the electrode potential increases, showing a well discernible curvature in the potential region of hydroxide adsorption.

The isotropic term A is generally proportional to the electrostatic field $\mathbf{E}_{DC}$ at the interface due to third-order nonlinear effects [21, 35]:

$$A = A^{(2)} + A^{(3)} E_{DC}, \tag{6}$$

where E_{DC} is the normal component of the interfacial field. As this in turn is proportional to the metal charge divided by the double layer dielectric constant: $E_{DC} \propto \sigma_{Me}/\varepsilon_{DL}$, the isotropic term can be proportional to the metal charge if ε_{DL} remains constant in a given potential interval. In a previous study we compared the isotropic term A with the charge on the metal electrode, which was calculated by integration of the current assuming no charge transfer from the adsorbate (F^- and/or OH^-) to the metal [20]. In the OH^- adsorption region, A was found to be proportional to the charge. This points to the validity of the assumption of little or no charge transfer between specifically adsorbed anions and the metal. Indeed, if we make the opposite assumption of full discharge of the anions upon adsorption, the charge computed by integration of the positive sweep of the CV will considerably exceed the charge on the metal. This will break the proportionality observed in the experiment. Such a case is indeed observed in region (b), where the faradaic process of surface oxide formation sets in (see Fig. 4 here and Fig. 4 of ref. [20]).

Fig. 4(b) shows the results for Ag(111) in a mixed 0.1 M NaF + 1 mM NaOH (pH $= 11$) electrolyte. It is remarkable that the behavior of the A and D terms *vs.* potential is essentially the same in this system as in the pure NaOH electrolyte, as given in Fig. 4(a), and also pure NaF electrolyte at pH $\simeq 8.3$ (not shown). Fig. 4(c) shows the same experiment for Ag(111) in acidic NaF + HF electrolyte at pH $= 5.8$.

In the potential region of anion adsorption (a), the dependence of A on the potential is similar in all electrolytes investigated, see upper panels of
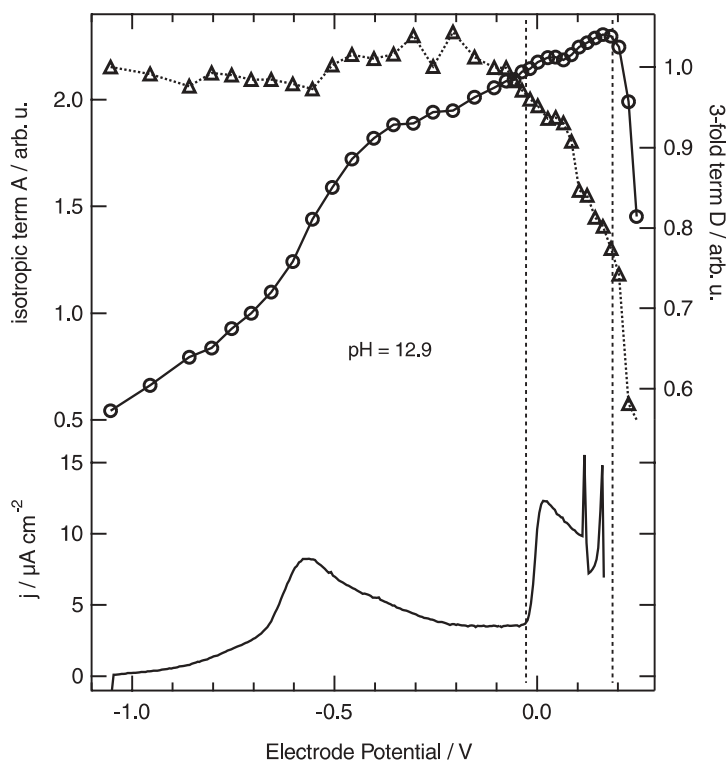
Fig. 4a. SHG isotropic (*A*) and threefold term (*D*) (upper panel) and anodic current density scan (lower panel) of Ag(111) in 0.1 M NaOH (pH = 12.9). The isotropic term is normalized to its value at −0.7 V, as it is assumed that near the point of zero charge, the interfacial fields are comparable in all systems. The 3-fold term is normalized to its starting value at −1.05 V. The dashed lines indicate the beginning of the underpotential oxidation region and the potential where *A* drops steeply.

Figs. 4(a) to 4(c). In each case, the isotropic term *A* displays a general increase as a function of electrode potential. In addition, there is a broad S-shape curvature feature coinciding with the adsorption of anions from the solution, as seen in the anodic scan of the CV (lower panels). Since *A* is proportional to the interfacial field [21], this shows that the field across the interface develops in the same manner in pure NaF/HF electrolyte as in pure NaOH electrolyte solution. Hence it can be concluded that the adsorption processes of F$^-$ and OH$^-$ at the Ag(111) surface are very similar. This gives further evidence that hydroxide, too, adsorbs without noticeable charge transfer. In this work we have not observed a minimum in the isotropic term around E_{pzc}. This is in line with a recent publication by Schmickler *et al.* [19]. Indeed these authors have proven both experimentally and theoretically that the isotropic contribution at Ag(*hkl*) electrodes exhibits a minimum *below* E_{pzc}.
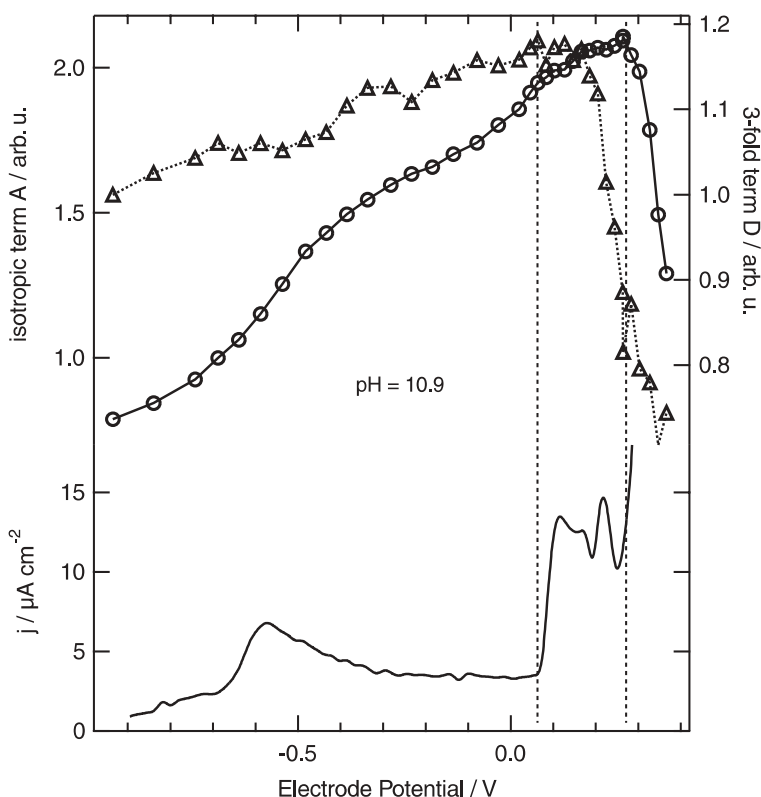
Fig. 4b. SHG isotropic (A) and threefold term (D) (upper panel) and anodic current density scan (lower panel) of Ag(111) in 1 mM NaOH + 0.1 M NaF (pH = 10.9). The isotropic term is normalized to its value at -0.68 V. The 3-fold term is normalized to its starting value at -0.94 V. The dashed lines indicate the beginning of the underpotential oxidation region and the potential where A drops.

   In Figs. 4(a) and (b), as the potential is moved into the region of surface oxide formation, the A term saturates and the 3-fold term D drops down. As was argued in [6, 20] on the basis of SHG, XPS and potential step experiments, the steep drop of the 3-fold term D in the positive-going direction of the potential can be explained by 2D islands of Ag_2O silver oxide growing on the surface. As the islands merge into a full monolayer, 3D oxide growth starts and causes the isotropic term A to decrease starting from approximately 190 mV (pH = 13) and 260 mV (pH = 11).

   In slightly acidic solution (Fig. 4(c), pH = 5.8) however, the situation is rather different. The anodic end of the current-potential characteristic (bottom panel) clearly shows the dissolution wave of silver. When the Ag(111) dissolution starts (at around 300 mV), the 3-fold term D drops.
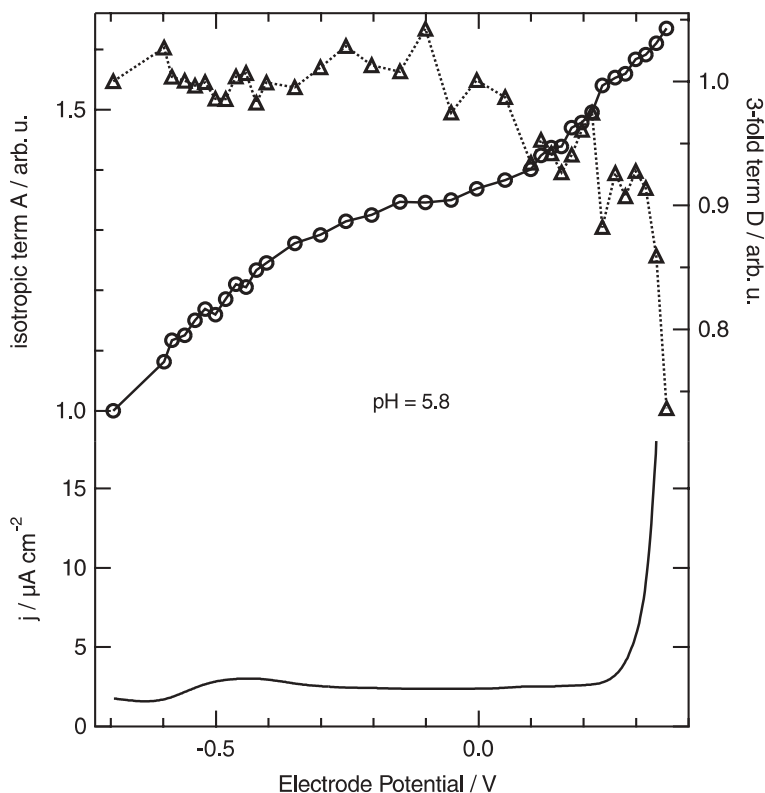
Fig. 4c. SHG isotropic (*A*) and threefold term (*D*) (upper panel) and anodic current density scan (lower panel) of Ag(111) in NaF + HF electrolyte (pH = 5.8). The isotropic and threefold terms are normalized to their starting values at −0.7 V.

The Ag/Ag$^+$ pair is characterized by a very high standard exchange current density of $j_{00} = 13.4$ A cm^{-2} with a charge-transfer coefficient of $\alpha = 0.65$ [36]. Assuming the dissolution reaction establishes the equilibrium concentration of Ag$^+$, we estimate from $E^0(\text{Ag/Ag}^+) = 0.799$ V $+ 0.059$ V $\times$ lg[Ag$^+$] [37] that the Ag$^+$-concentration at 340 mV(HgO) is approximately [Ag$^+$] = 10^{-5} mol/l. For this concentration, the exchange current density is $j_0 = 7.5 \times 10^{-3}$ A cm^{-2}; at one electron per surface atom, this yields an atom exchange rate of 4.7×10^{16} atoms cm^{-2} s^{-1}. The (111) surface of silver contains 1.38×10^{15} atoms cm^{-2}, hence at 0.34 V, approximately 34 monolayers of silver are dissolved and deposited each second. For more positive potentials, this rate increases by a factor of 4.5 every 60 mV. This high exchange rate will clearly lead to a substantial degree of disorder in the topmost surface layers, which causes the 3-fold symmetry of the surface to be disturbed, hence the decrease in *D*. Meanwhile, the isotropic contribution continues rising even

under dissolution potential, showing the absence of oxide formation. Only at very high potentials (positive of 440 mV, not shown), there is a slight decrease in A which points to a lower polarizability as a consequence of prolonged Ag dissolution.

The similarity in the SHG data between NaF and NaOH electrolytes is quite remarkable. The experiments show that while the interaction of Ag(111) with OH$^-$ is stronger than with F$^-$, the adsorption mechanism, and thus the structure of the interfacial layer between Ag(111) and OH$^-$ or F$^-$ containing aqueous electrolytes is similar. Neither of the adsorption processes involves noticeable charge transfer. Only as the potential is increased further, OH$^-$ is discharged and transformed into ionic oxygen interacting strongly with the Ag surface. This result is at variance with conclusions in the literature [22] suggesting the transfer of one electron per OH$^-$ upon adsorption.

Fluoride ions in aqueous solutions are strongly hydrated. According to calculations, F$^-$ hydration shells consist of 17.4 water molecules divided into 6.0 water molecules in the primary and 11.4 in the secondary shell [38]. The strong hydration of fluoride is usually supposed to prevent its specific adsorption. Doubova *et al.* [30] have therefore ascribed the surface activity of F$^-$ at Ag single crystal surfaces to the weakness of the interaction between Ag and H$_2$O (low hydrophilicity), rather than to specific chemical interactions of F$^-$ with the Ag surface. This may account for a negative free energy of the reaction:

$$Ag - H_2O + F^-(sol) \rightarrow Ag - F^- + H_2O(sol) , \qquad (7)$$
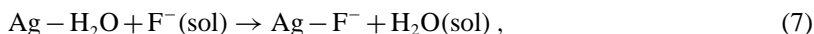
where F$^-$(sol) and H$_2$O(sol) designate F$^-$ and H$_2$O in the solution bulk. Indeed, UHV studies confirm that water interacts with clean Ag surfaces very weakly and is desorbed in a single peak as multilayer water at 160 K (see [39] and refs. therein). Recent molecular dynamics simulations show that as a consequence of the interplay between hydration and adsorption, contact adsorption of ions is possible even without specific interactions between ions and metal surfaces [40].

In UHV simulations of the electric double layer at Ag(110), Stuve *et al.* have proved that co-adsorbed fluoride exerts a strong stabilizing effect on surface water through hydrogen bonding [41, 42]. It was shown that in the case of even small amounts of fluoride present on the surface, the thermal desorption of water exhibits four distinct states desorbing at higher temperatures (190 K to 270 K) compared to water desorbing from a clean surface (162 K). While pure interfacial water did not show any order in LEED, fluoride induced some ordering of the co-adsorbate layer [41]. This indicates that the hydration of F$^-$ leads to a significant lateral structuring of the double layer. Vertical structure, *i.e.* ordering of the water molecules in layers which are parallel to the surface was found by Toney *et al.* on Ag(111) in 0.1 M NaF electrolyte using surface X-ray scattering [43]. The layering effect was found to be potential-dependent, with the distance from the surface to the first water layer being smaller positive

of the point of zero charge, which complies with current views of the electrode-water interface. Theoretical modelling confirms layering of the interfacial water [44] and its dependence on the charge density at the metal surface (see also [45]). However, these studies have so far been unable to account for the unexpectedly high density of water molecules in the inner layer, which, according to the X-ray scattering data of Toney *et al.* exceeded that in the solution bulk by nearly a factor of 2 above the point of zero charge. Given Stuve's observation that the number of water molecules per hydrated F^- is exceptionally large at very low F^- coverages [41], one might assume that the hydration characteristics of fluoride is responsible for the high water densities in the inner layer.

In the UHV double-layer simulations [41], it is found experimentally that at low F^- coverage, the number of water molecules in the hydration shell of a single fluoride ion can be as high as 13, indicating the formation of a second hydration shell. In connection with the respective intermediate desorption temperature, the authors conclude that long range interactions lead to correlations between fluoride ions through their hydration shells. Hydrogen bonds have proved to be the driving mechanism of lateral ordering [41, 42]. Even though the effect is weaker for OH^-, its influence on the double layer structure is comparable [41]. Hydroxide, being isoelectronic with F^-, interacts with co-adsorbed water at a Ag(110)/UHV interface in a remarkably similar manner in terms of adsorption sites, hydrogen bonding and desorption temperatures [46].

Based on the information provided by these UHV studies and our experimental observations we propose that the adsorption of both F^- and OH^- ions is a consequence of the interplay of (i) weak specific interactions between the Ag(111) surface and these ions, (ii) the weakness of the interaction of Ag(111) with H_2O and (iii) lateral interactions between the anions and water molecules through hydrogen bonding. These may reach further than the hydration shell of each ion, leading to long-range stabilization effects. An ordered overlayer may be formed, where co-adsorbed fluoride and hydroxide ions interact with each other through hydrogen bonding to water molecules rather than by chemical interaction with the Ag substrate. It is interesting to note here that in surface-enhanced Raman-scattering experiments on silver, Fleischmann and Hill have found a strong influence of the alkali metal cation on the vibrational spectra [47]. It was concluded that the strongly solvated cations co-adsorbed with specifically adsorbed anions exert stabilizing effects on the inner double layer. Clearly, a full model of a structured inner layer would have to include specifically adsorbed anions, water molecules and co-adsorbed cations.

4. Conclusions

In mixed NaF/NaOH electrolytes, the anion adsorption at Ag(111) at different pH values shows a cross-over from OH^--dominated (very alkaline solutions) to F^--dominated adsorption (neutral and acidic solutions). At intermediate pH

values, both ion types are present in the adsorbate layer. Neither fluoride nor hydroxide is discharged upon adsorption.

The sub-monolayer oxidation occurring below the reversible Ag/Ag_2O oxidation potential proceeds from adsorbed OH species; the OH^- content in the ionic adlayer saturates at very high bulk OH^- concentration (pH $= 14$).

The analysis of the SHG anisotropy shows remarkable similarities between pure and mixed NaF/NaOH electrolytes. The isotropic term A reveals that adsorption of pure F^- and OH^- as well as co-adsorption of both ions proceeds the same way, pointing to both ions being specifically adsorbed. The SHG data give further evidence that in all cases, the adsorbed ions retain their negative charge up to potentials where oxidation sets in. In the case of acidic electrolyte, where no OH^- ions are present at the surface, the SHG data show characteristics of Ag dissolution.

From comparison with previous works on the simulation of an electric double layer in UHV experiments, we infer that lateral interactions between the ions, mediated by H-bonding, have an important impact on adlayer formation during co-adsorption of fluoride and hydroxide.

Acknowledgement

References

1. S. Strbac and R. R. Adžić, J. Electroanal. Chem. **337** (1992) 355.
2. S. Strbac and R. R. Adžić, J. Electroanal. Chem. **403** (1996) 169.
3. A. G. Kicheev and V. M. Sheblovinskii, Electrokhimiya **19** (1983) 1071.
4. M. Honda, T. Kodera, and H. Kita, Electrochim. Acta **28** (1983) 727.
5. E. R. Savinova, S. Wasle, and K. Doblhofer, Electrochim. Acta **44** (1998) 1341.
6. E. R. Savinova, A. Scheybal, M. Danckwerts, U. Wild, B. Pettinger, K. Doblhofer, R. Schlögl, and G. Ertl, Faraday Discussions **121** (2002) 181.
7. T. P. Dirske, J. Electrochem. Soc. **106** (1959) 920.
8. R. D. Giles, J. A. Harrison, and H. R. Thirsk, J. Electroanal. Chem. **22** (1969) 375.
9. J. M. M. Droog and F. Huisman, J. Electroanal. Chem. **115** (1980) 211.
10. M. Lopez Teijelo, J. R. Vilche, and A. J. Arvia, J. Electroanal. Chem. **131** (1982) 331.
11. M. Lopez Teijelo, J. R. Vilche, and A. J. Arvia, J. Appl. Electrochem. **18** (1988) 691.
12. C. Alonso, R. C. Salvarezza, J. M. Vara, and A. J. Arvia, Electrochim. Acta **35** (1990) 489.
13. D. Y. Zemlyanov, E. Savinova, A. Scheybal, K. Doblhofer, and R. Schlögl, Surf. Sci. **418** (1998) 441.
14. E. R. Savinova, D. Zemlyanov, A. Scheybal, Th. Schedel-Niedrig, K. Doblhofer, and R. Schlögl, Langmuir **15** (1999) 6546.

15. E. R. Savinova, D. Y. Zemlyanov, A. Scheybal, R. Schlögl, and K. Doblhofer, Langmuir **15** (1999) 6552.
16. Sh. K. Shaikhutdinov, E. R. Savinova, A. Scheybal, K. Doblhofer, and R. Schlögl, J. Electroanal. Chem. **500** (2001) 208.
17. E. R. Savinova, P. Kraft, B. Pettinger, and K. Doblhofer, J. Electroanal. Chem. **430** (1997) 47.
18. E. R. Savinova, D. Y. Zemlyanov, B. Pettinger, A. Scheybal, R. Schlögl, and K. Doblhofer, Electrochim. Acta **46** (2000) 175.
19. G. Beltramo, E. Santos, and W. Schmickler, J. Electroanal. Chem. **447** (1998) 71.
20. M. Danckwerts, E.R. Savinova, B. Pettinger, and K. Doblhofer, Appl. Phys. B **74** (2002) 635.
21. B. Pettinger, C. Bilger, J. Lipkowski, and W. Schmickler, in *Interfacial Electrochemistry*; A. Wieckowski, ed. by Marcel Dekker, New York (1999), pp. 373–404.
22. B. M. Jovic, V. D. Jovic, and G. R. Stafford, Electrochem. Commun. **1** (1999) 247.
23. K. J. Stevenson, X. Gao, D. Hatchett, and H. S. White, J. Electroanal. Chem. **447** (1998) 43.
24. N. S. Marinković, J. S. Marinković, and R. R. Adžić, J. Electroanal. Chem. **467** (1999) 291.
25. G. Valette and A. Hamelin, J. Electroanal. Chem. **45** (1973) 301.
26. G. Valette, A. Hamelin, and R. Parsons, Z. Phys. Chem. NF **113** (1978) 71.
27. A. Hamelin, E. S. Sevastyanov, T. Vitanov, and A. Popov, J. Electroanal. Chem. **145** (1983) 225.
28. G. Valette, J. Electroanal. Chem. **269** (1989) 191.
29. M. Bacchetta, S. Trasatti, L. Doubova, and A. Hamelin, J. Electroanal. Chem. **255** (1988) 237.
30. L. Doubova and S. Trasatti, Electrochim. Acta **42** (1997) 785.
31. T. Vitanov, A. Popov, and E. S. Sevastyanov, J. Electroanal. Chem. **142** (1982) 289.
32. *Encyclopedia of Electrochemistry*, ed. by A. J. Bard and M. Stratmann, Vol. 1, *Thermodynamics and Electrified Interfaces*, Vol. ed. by E. Gileadi and M. Urbakh, Wiley-VCH, Weinheim (2002).
33. A. Kolics and A. Wieckowski, J. Phys. Chem. **105** (2001) 2588.
34. P. Delahay, M. Pourbaix, and P. Van Rysselberghe, J. Electrochem. Soc. **98** (1951) 65.
35. P. Guyot-Sionnest and A. Tadjeddine, J. Chem. Phys. **92** (1990) 734.
36. C. H. Hamann and W. Vielstich, *Elektrochemie* 3rd ed., Wiley VCH Weinheim, 1998, Ch. 4.
37. M. Pourbaix, N. de Zoubov, and J. van Muylder, *Atlas d'Equilibres Electrochimiques*, Gauthier-Villars, Paris (1963).
38. J. N. Glosli and M. Philpott, J. Chem. Phys. **98** (1993) 9995.
39. P. A. Thiel and T. E. Madey, Surf. Sci. Rep. **7** (1987) 211.
40. E. Spohr, Electrochim. Acta **44** (1999) 1697.
41. A. Krasnopoler and E. M. Stuve, Surf. Sci. **303** (1994) 355.
42. A. Krasnopoler, A. L. Johnson, and E. M. Stuve, Surf. Sci. **328** (1995) 186.
43. M. F. Toney, J. N. Howard, J. Richer, G. L. Borges, J. G. Gordon, O. R. Melroy, D. G. Wiesler, D. Yee, and L. B. Sorensen, Surf. Sci. **335** (1995) 326.
44. J. W. Halley, S. Walbran, and D. L. Price, in *Interfacial Electrochemistry*, ed. by A. Wieckowski, Marcel Dekker, New York (1999), p. 1; M. L. Berkowitz, I.-C. Yeh, E. Spohr, *ibid*, p. 33.
45. D. L. Price, J. Chem. Phys. **112** (2000) 2973.
46. K. Bange, T. E. Madey, J. K. Sass, and E. M. Stuve, Surf. Sci. **183** (1987) 334.
47. M. Fleischmann and I. R. Hill, J. Electroanal. Chem. **146** (1983) 367.